

MODELS FOR THE EFFECTS OF G-SEAT CUING
ON ROLL-AXIS TRACKING PERFORMANCE

William H. Levison
Bolt Beranek and Newman, Inc.
10 Moulton Street
Cambridge, MA 02238

Grant R. McMillan
Air Force Aerospace Medical Research Laboratory
Wright-Patterson AFB, Ohio 45433

Edward A. Martin
USAF Aeronautical Systems Division
Wright-Patterson AFB, Ohio 45433

submitted to the
20th Annual Conference on Manual Control
June 12-14, 1984, NASA-ARC, California

ABSTRACT

Including whole-body motion in a flight simulator improves performance for a variety of tasks requiring a pilot to compensate for the effects of unexpected disturbances. A possible mechanism for this improvement is that whole-body motion provides high derivative vehicle state information which allows the pilot to generate more lead in responding to the external disturbances. In developing new motion simulation algorithms for an advanced g-cuing system we were, therefore, surprised to discover that an algorithm based on aircraft roll acceleration produced little or no performance improvement. On the other hand, algorithms based on roll position or roll velocity produced performance equivalent to whole-body motion. This paper describes the analysis and modeling conducted at both the sensory system and manual control performance levels to explain the above results.

INTRODUCTION

The Air Force Aerospace Medical Research Laboratory and the Aeronautical Systems Division are jointly investigating motion and force cuing alternatives to whole-body motion. This paper summarizes the progress on an investigation of the capability of an advanced g-cuing system to provide rotational motion information to a pilot performing a flight control task. Human performance modeling is being conducted to explore hypotheses concerning the underlying sensory and performance mechanisms.

METHODS

Motion Cuing Devices

Two motion cuing devices were used: (1) the Advanced Low Cost G-Cuing System (ALCOGS), and (2) the Roll-Axis Tracking Simulator (RATS). The ALCOGS includes hydraulically-actuated seat pan, backrest, and seat belt elements mounted in an aircraft seat frame [1]. In the studies reported here, the one-piece seat pan was the only active cuing element. The RATS is a whole-body, roll-axis motion device. The axis of rotation is through the buttocks of the subject.

Drive Algorithm Development

Pressure Matching Algorithm. The initial approach was to develop a means of driving the ALCOGS seat pan such that the pressure produced on the human buttocks matched those one would experience in the RATS. Using small force-sensing strain gauges located under the ischial tuberosities of the buttocks, we measured the pressures produced by sinusoidal roll motion in the RATS. A multiple regression performed on data collected over a range of amplitudes and frequencies suggested that buttocks pressures were a function of RATS roll angle and roll acceleration:

$$PSI_{\text{Buttocks}} = -.064 \phi_{\text{RATS}} + .0042 \ddot{\phi}_{\text{RATS}} \quad (1)$$

where PSI = pressure in lbs/in^2 , ϕ = roll angle in deg, and $\ddot{\phi}$ = roll acceleration in deg/sec^2 . For data collected under a similar sinusoidal motion in the ALCOGS, buttocks pressures were a simple function of seat pan roll angle:

$$PSI_{\text{Buttocks}} = .081 \phi_{\text{ALCOGS}} \quad (2)$$

Setting the equations equal to one another and solving for the ALCOGS seat pan angle (in deg) results in the following pressure matching algorithm:

$$\phi_{\text{ALCOGS}} = K(-.79 \phi_{\text{RATS}} + .052 \ddot{\phi}_{\text{RATS}}) \quad (3)$$

K values only up to 0.4 (40% of RATS pressures) were used to prevent the ALCOGS seat pan from striking its limits of travel.

The results obtained while testing this algorithm (see Primary Data Reduction Section), suggested that drive algorithms based on the separate derivatives of roll motion would be of

interest. Therefore, the following algorithms were also developed.

Single Derivative Algorithms. Pure position (Equation 4) and pure acceleration (Equation 5) algorithms were derived by setting either the acceleration or position coefficient of Equation 3 to zero. Since matching buttocks pressure was not a concern here, the equations are shown below in terms of the simulated aircraft motion parameters:

$$\phi_{\text{ALCOGS}} = .02 \ddot{\phi}_{\text{Simulated Aircraft}} \quad (4)$$

$$\phi_{\text{ALCOGS}} = \pm .32 \phi_{\text{Simulated Aircraft}} \quad (5)$$

where ϕ = roll angle in deg, and $\ddot{\phi}$ = roll acceleration in deg/sec². As shown in Equation 5, both sign relationships were investigated with the position algorithm.

A velocity algorithm was also developed in which ALCOGS seat pan angle was made proportional to simulated aircraft roll velocity:

$$\phi_{\text{ALCOGS}} = \pm .23 \dot{\phi}_{\text{Simulated Aircraft}} \quad (6)$$

where $\dot{\phi}$ = roll velocity in deg/sec. Both sign relationships were investigated with this algorithm, as well.

Drive Algorithm Testing

The utility of the algorithms was evaluated by comparing human performance on a roll-axis tracking task under static (visual cue only) and g-seat motion conditions (visual and g-seat cues). The visual display consisted of an aircraft symbol and a dotted reference line which subtended a 9 deg field-of-view. The task was to maintain zero roll angle (keep the symbol and reference aligned) in the presence of strong turbulence using a side-mounted, force-sensing control stick.

The roll dynamics were represented by the transfer function:

$$V(s) = 16 \cdot \frac{5}{s+5} \cdot \frac{20}{s+20} \cdot \frac{1}{s} e^{-.072s} \quad (7)$$

At very low frequencies, a control input of one pound produced a simulated roll rate of 16 deg/sec. The lag at 5 rad/sec represents the roll response of a fighter-type aircraft; the lag at 20 rad/sec approximates the response of the moving-base

simulator; and the delay of 0.072 seconds represents the combined effects of digital frame time, sample-and-hold, antialiasing filters, plus the effective delay of the g-seat hydraulic and servo systems. (Regardless of whether a subject was performing the tracking task in the ALCOGS or RATS under static or visual plus motion conditions, the dynamics and delays were identical).

The external forcing function was generated as a sum of thirteen sine waves, with frequencies and amplitudes selected to approximate a random disturbance process having a power spectral density of the form:

$$\Phi_{ii} = \frac{K}{(s+2)^2} \quad (8)$$

and an rms value of .88 pounds equivalent control force. The sinusoids were randomly phased with respect to each other, and from trial-to-trial, to minimize the predictability of the disturbance waveform. This forcing function added to the pilot's control input and thus served as a direct disturbance to vehicle roll angle.

Under g-seat motion conditions the seat pan of the ALCOGS was driven in roll using Equations 3-6. Because the research reported here consisted of a series of pilot studies, the "experimental design" included both within and between subject treatments and the number of subjects in each algorithm group was not the same. (See Table 1, below). With the exception of the acceleration algorithm, the data for each group represents asymptotic performance after 32 or more 3 minute training trials conducted over several days. In all cases, mean-squared or root-mean-squared (RMS) tracking error was provided to the subjects after each trial.

The tracking performance data collected under whole-body motion in the RATS also represented asymptotic performance. The task dynamics, visual display, control stick, etc. were identical to those used in the ALCOGS. The RATS drive algorithm, however, matched the roll angle of the simulated aircraft in a 1:1 fashion.

PRIMARY DATA REDUCTION

Formal analysis was performed on data obtained under the following cuing conditions:

- a. "Static" (visual display of roll angle error; no ALCOGS motion)
- b. "Position" (visual plus ALCOGS seat pan angle proportional to simulated aircraft roll angle)

- c. "Velocity" (visual plus ALCOGS seat pan angle proportional to simulated aircraft roll velocity)
- d. "Acceleration" (visual plus ALCOGS seat pan angle proportional to simulated aircraft roll acceleration)
- e. "Combined" (visual plus ALCOGS seat pan angle proportional to a linear combination of simulated aircraft roll angle and roll acceleration).

Error standard deviation (SD) scores were computed for each data trial.* These scores were averaged across trials for each subject; the subject means were then averaged to yield group means for each experimental condition. Table 1a shows, for each cuing condition, the average tracking error SD score, the standard deviation of the subject means, and the number of subjects providing data. Note that the inter-subject variability was less than 20% of the group mean, even for the conditions with only two subjects.

The acceleration and combined algorithms yielded a modest reduction in the tracking error score (about 15%) compared to static performance. On the other hand, the position and velocity algorithms yielded reductions of about 50% and 65%, respectively, and were essentially equivalent to performance in the RATS (mean RMS error = 2.3 degrees).

Differences between pairs of group means were tested for statistical significance by means of a t-test appropriate to unequal sample sizes. Differences significant at an alpha level greater than 0.05 are considered "not significant" for this discussion. Table 1b shows that the mean error SD scores obtained for the position and velocity cuing conditions were significantly different from each other and from the scores obtained for the remaining cuing conditions. Differences among the static, acceleration, and combined conditions were generally not significant.

Effects of g-seat cuing on operator frequency response are shown in Figure 1; position and velocity cuing are compared with static in Figure 1a, whereas acceleration and combined cuing effects are shown in Figure 1b. A value of zero dB for the amplitude ratio ("gain") represents one pound of control force per degree of roll angle error; zero dB remnant signifies 1 pound² of control power per radian/second.

*Because the forcing function was a zero-mean process, the error SD score is approximately equal to the RMS tracking error.

TABLE 1. ANALYSIS OF THE TRACKING ERROR SD SCORES

a) Group Means

cuing	Mean	Std Dev	Subjects
Static	6.0	0.51	6
Position	3.0	0.50	6
Velocity	2.1	0.20	6
Acceleration	5.2	0.99	2
Combined	4.8	0.21	2

b) Alpha Level of Significance

	Posn.	Vel.	Accel.	Comb.
Static	.001	.001	--	.05
Position		.01	.01	.01
Velocity			.001	.001
Acceleration				--

-- Alpha > 0.05.
2 trials/subject.

a) Position and Velocity Algorithms

b) Acceleration and Combined Algorithms

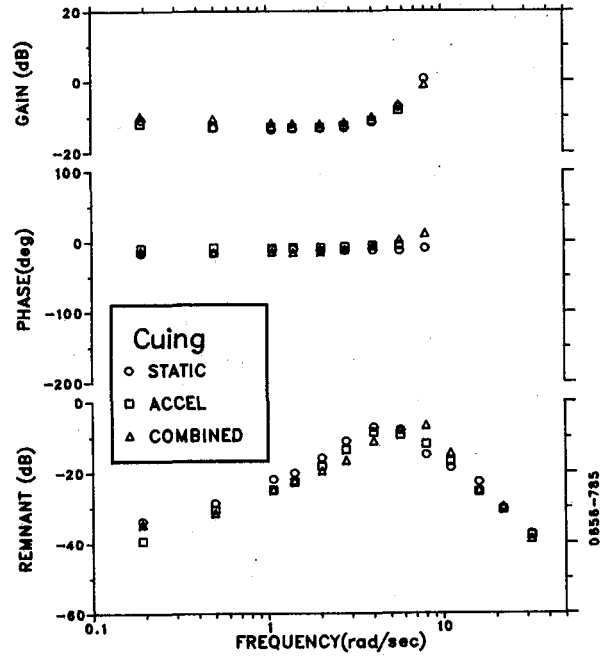
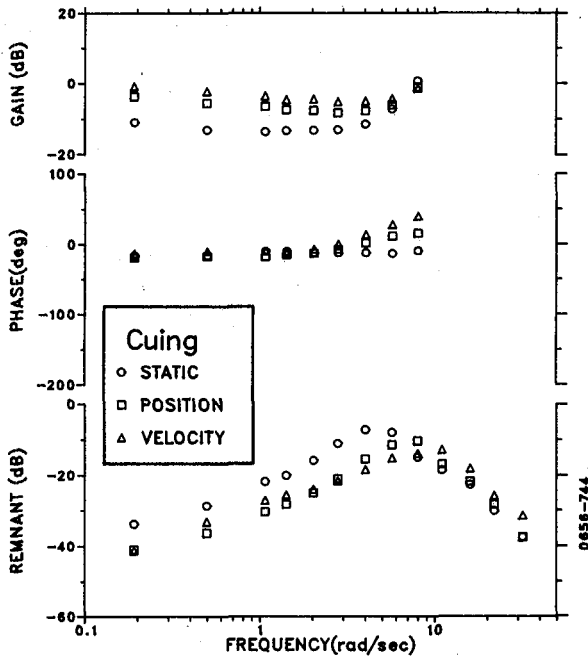


Figure 1. Effect of Cuing on Operator Frequency Response
Average of 2-6 subjects, 2 trials/subject

G-seat cuing with the position drive algorithm yielded larger operator gain at low frequencies, more phase lead at high frequencies, and less remnant at low frequencies. The velocity drive law yielded even larger gain and phase lead, and a remnant spectrum comparable to that of the position drive law. The acceleration and combined drive algorithms had much smaller effects on the frequency response. Overall, the frequency response trends shown in Figure 1 are consistent with the trends of the tracking error scores.

A follow-up experiment indicated that the subjects could perform the tracking task with positional ALCOGS cuing alone (i.e., no visual cues), and that error scores were nearly as low (mean RMS error = 3.7 degrees) as those obtained with concurrent ALCOGS and visual cuing.

In summary, the following experimental trends were revealed by the study on g-seat cuing:

1. A modest reduction in tracking error score with either the acceleration or the combined acceleration and position drive laws.
2. Substantially improved performance with the position and velocity g-seat drive laws.
3. Lower tracking error scores with velocity than with position cuing.
4. Ability to track almost as well with position g-cuing alone (i.e., no visual cuing) as with combined visual and position g-cuing.

MODEL ANALYSIS

Model analysis of the foregoing experimental results was conducted as part of the overall goal of developing a theoretical framework for predicting the pilot's use of combined visual and non-visual cues. A concurrent and more specific goal was to develop a model for the psycho-physiological mechanisms responsible for the observed relationship between g-seat cuing algorithm and tracking performance. The optimal control model (OCM) for pilot/vehicle systems was used for this analysis.

Model Description

The reader is assumed to be familiar with the general structure of the OCM. Figure 2 shows a block diagram of the task environment as modeled for this analysis. The first block contains the equations of motion of the simulated aircraft in the roll axis, plus the first-order approximation to the RATS dynamics. Six "outputs", (perceptual quantities) are considered:

tracking error and error rate for visual perception, and tracking error, error rate, error acceleration, and error acceleration rate for haptic cuing. The visual outputs are delayed by 0.072 seconds (approximated in the model formulation by a first-order Pade) to mimic the delays present in the laboratory simulation. The delayed outputs e_v and $e_{\dot{v}}$ represent the visual cues acted on by the pilot model.

The remaining four outputs of the dynamics block are processed by the g-seat drive algorithm, a second-order model of the g-seat dynamics, and a lead-lag model for mechanoreceptor transduction. To be consistent with our treatment of visual-cue processing, we assume that the pilot perceives both the primary receptor output "m" and its first derivative "m". We shall refer to these two cues as the "motion cues".

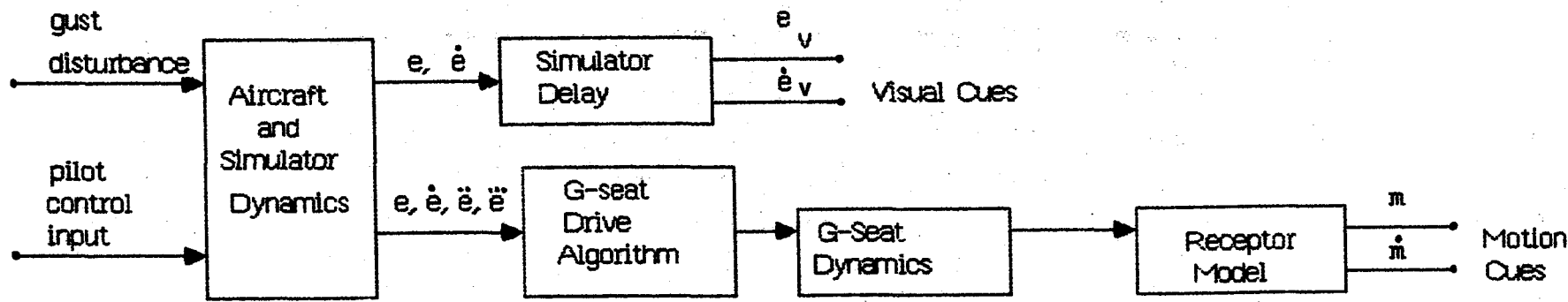
Relevant physiological and psychological literature was reviewed in order to derive a math model for transduction of haptic cues [2-19]. This literature covered a variety of receptor types, biological species, and experimental preparations. Consequently, the lead-lag model shown in Figure 2 does not reflect a particular sensory mechanism, but rather an average effect of (presumably) multiple mechanisms involved in the sensory process.

On the basis of largely qualitative information, we derived a lead-lag model for receptor response having a pole at 5 rad/sec (based on the minimum 0.2 second time constant found in the literature search) and a zero at 0.5 rad/sec (an educated guess based on published time histories). Lacking any meaningful data on bandwidth limitations, we did not associate any low-pass characteristics with this receptor model.

There is some psychophysical evidence to indicate that the human's reaction time to haptic stimuli are about 40 msec less than the reaction time to visual stimuli [18,19]. The formulation shown in Figure 2 accounted for this difference.

The only task-to-task variation relevant to the model of Figure 2 was the drive algorithm, which was changed to match the form of the experimental drive algorithm. The position, velocity, and acceleration drive algorithms were modeled as unity gains on either error, error rate, or error acceleration; and the combined algorithm was represented as an appropriately weighted sum of error and error acceleration. Since the experimental drive algorithms were considered sufficient to provide g-seat cuing well above sensory threshold levels, perceptual thresholds were not considered in this modeling exercise, and "display" scaling was therefore unimportant.*

*The OCM will scale its response strategy optimally with regard to display scaling.



Simulator Delay: Pade Approximation to T=0.072 seconds

G-Seat Dynamics:

$$\frac{47.1^2}{S^2 + 1414(47.1)S + (47.1)^2}$$

Receptor Model:

$$\frac{S + 0.5}{S + 5}$$

Figure 2. Model for System Dynamics and Displays

743

Independent model parameters relating to inherent limitations of the human operator were selected in a manner consistent with previous application of the OCM to laboratory tracking tasks. The following "nominal values" were assigned:

- o time delay for visual cues: 0.2 seconds
- o motor time constant: 0.1 second
- o observation noise/signal ratio for visual cues: -20 dB
- o motor noise/signal ratio: -50 dB

In addition, observation noise/signal ratios of -22.7 dB were assigned to the two motion cues to provide a good match to the tracking error score obtained with the position drive algorithm; this noise/signal ratio was maintained for analysis of the remaining cuing algorithms.

While Figure 2 may reflect a new way of treating g-seat cuing, it does not imply a change in the basic structure of the human operator model. That is, the relationships shown in Figure 2 were implemented within the existing OCM by appropriate definitions of systems dynamics and display variables -- no changes to the computer program were required.

We refer to the model of Figure 2 as the "receptor model" in the sense that it includes an explicit submodel for mechanoreceptor transduction. An alternative "noise model" was explored in which the receptor submodel was omitted and, instead, information provided by the g-seat was modeled directly. That is, the subject was assumed to perceive g-seat displacement and g-seat rate with associated observation noise/signal ratios of -15 dB and -25 dB, respectively.* As was the case with the receptor model, only the g-seat drive algorithm was changed from task-to-task; other independent parameters of the pilot model were held fixed for all experimental conditions.

The receptor and noise models are similar in that both present high-quality rate information related to g-seat motion and poor-quality displacement information. The receptor model accomplishes this quality differential by the way in which it linearly combines position and rate information. The noise model accomplishes a similar effect by assigning different perceptual noises to position and rate information. Because we assume that the subject perceives the first derivative of the receptor

*These noises were selected to provide a good match to the position-drive results.

output, the receptor model also provides g-seat acceleration information -- a quantity we have not included in the noise treatment.

Principal Model Results

Comparisons of model predictions with experimental tracking-error SD scores are shown in Figures 3a and 3b for the "receptor" and "noise" models, respectively. The solid symbols indicate the group means, and the vertical bars indicate the standard deviations of the subject means.

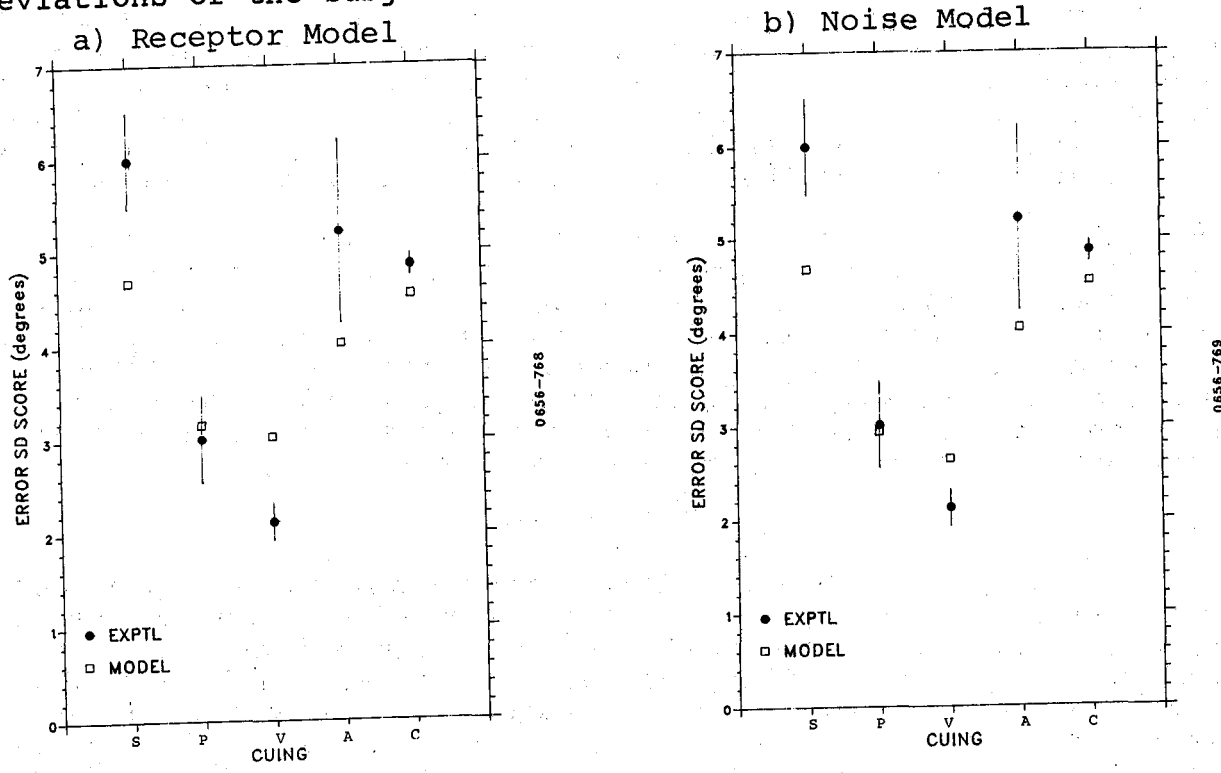


Figure 3. Effect of Cuing on Average Error SD Score
S = Static, P=Position, V=Velocity, A=Acceleration, C=Combined

The two model treatments yielded similar results, with the noise model providing slightly better matches to the position and velocity drive conditions. The model reproduced the major experimental trends: namely, that (1) position and velocity drive algorithms result in substantially improved performance compared to static tracking, and (2) the acceleration and combined algorithms result in only marginally improved performance relative to static.

Although not shown in Figure 3, the model also predicted that the subjects would be able to perform the task with position g-seat cuing alone (no visual cues), and that RMS error would be substantially lower than with visual cues only. This prediction agreed with the follow-up study.

There were some discrepancies between predicted and experimental results, however. Although the model predicted that the velocity algorithm would yield lower tracking errors than the position algorithm, the model underestimated the magnitude of this performance difference. The model also predicted that the acceleration algorithm would be superior to the combined algorithm, whereas the reverse trend was found experimentally. Finally, the model underestimated tracking errors for the more difficult configurations.

Predicted and measured operator frequency response are shown in Figure 4. To minimize clutter, data from the position and velocity conditions are shown in one graph, whereas acceleration and combined conditions are represented in another. For convenience, static response is plotted in all graphs. Predictions obtained with the receptor model are shown in Figures 4a and 4b; results of the noise model are given in 4c and 4d.

The two models predicted the same overall performance trends. They correctly predicted that the position and velocity cuing algorithms would have a greater influence on operator frequency response, compared to visual-only cuing, than would the acceleration and combined response. Furthermore, the effects of position and velocity cuing on operator gain and phase shift were matched in some detail. The rank ordering of the remnant response across cuing conditions was also predicted.

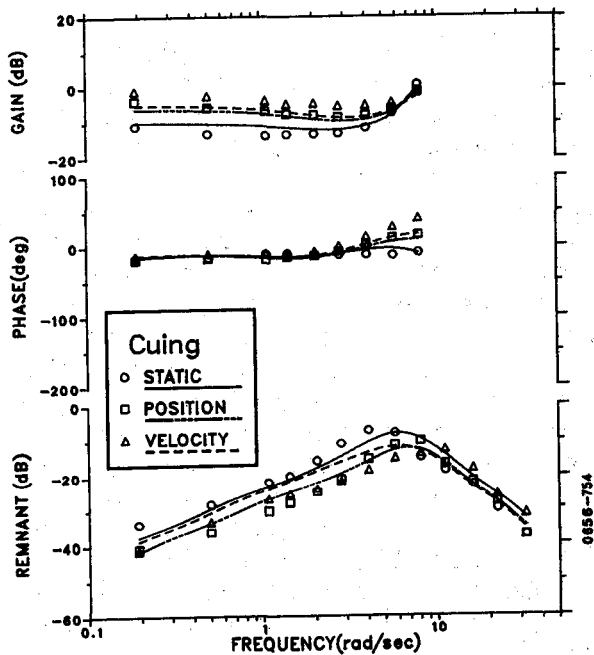
DISCUSSION

Overall, the modeling philosophies explored here provided a good match to the important trends of the experimental results. Specifically, they accounted for the large effects of position and velocity g-seat cuing, and the relatively small effects of acceleration and combined g-seat cuing, with a consistent set of independent model parameters. Whether or not this modeling philosophy can be generalized to other cuing algorithms and other types of motion (e.g., z-axis translational motion) remains to be determined. Of the various modeling philosophies explored in this study, the approach described here seems to be the most promising.

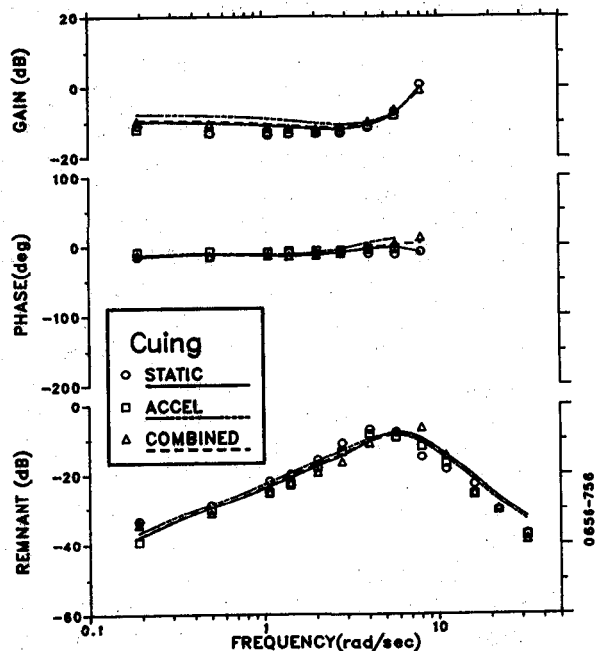
Additional analyses revealed appreciable performance differences between groups trained with the plus and minus sign on the position or velocity drive algorithms. (Tracking scores were substantially lower than static cuing for either sign

*The acceleration group was not trained to asymptote. Training curves indicate that this group, trained to asymptote, would have performed about the same as the group trained with the pressure-matching algorithm.

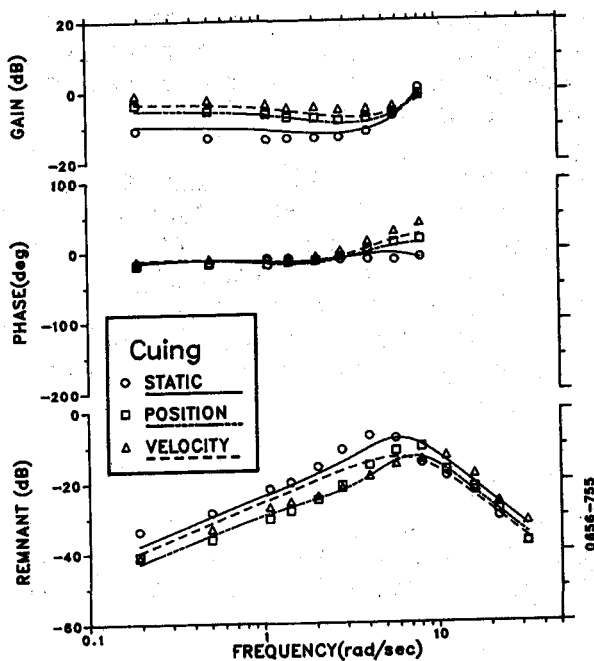
a) Receptor Model,
Posn & Vel Algorithms



b) Receptor Model,
Accel & Comb Algorithms



c) Noise Model,
Posn & Vel Algorithms



d) Noise Model,
Accel and Comb Algorithms

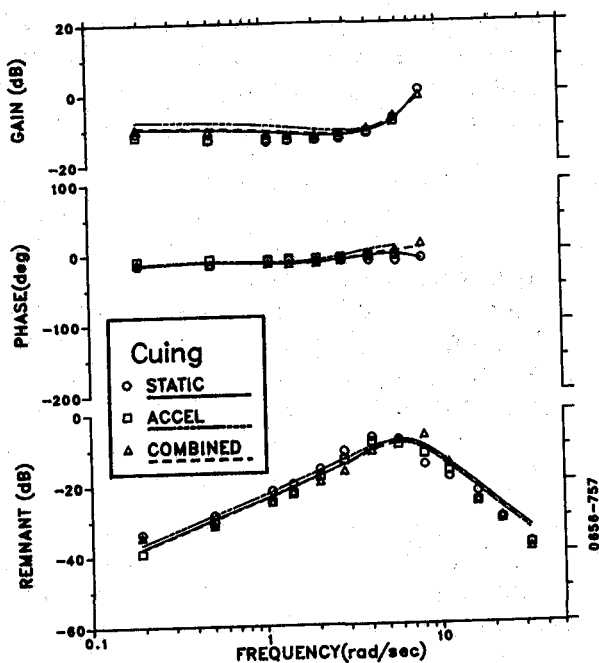


Figure 4. Effect of Cuing on Operator Frequency Response
Average of 2-6 Subjects, 2 trials/subject

convention, however.) Preliminary modeling suggested that these effects could be accounted for by appropriate modeling of biomechanical coupling between seat pan and control stick.

As we have noted, although gross trends were replicated, some of the finer details were not mimicked. To some extent, the performance compression seen in the model predictions may be due to the fact that, for this set of experiments, the model accounts for performance differences solely through task-related differences in perceptual cuing. Now, a recent review of a large body of experimental and model results suggests that, for systems having high-order response characteristics and/or significant delays, motion cuing may provide a double benefit [20]. First, the subject may be able to construct a more accurate "internal model" of system response dynamics than is possible with only visual cuing; and, second, motion-related cues allow more accurate state reconstruction because of high-derivative and/or low-noise information. Only the second factor has been considered in the model analysis presented here -- the current model analysis assumes a perfect internal model for all cuing conditions. Although the OCM is currently able to treat deficient internal models, further model development will be required if we are to predict how the operator's internal model is influenced by the cuing environment.

As mentioned earlier, because of the desire to explore training issues, different subject groups were used for the various experimental conditions. These groups did not all receive the same amount of training, and, in the case of the acceleration and combined-algorithm groups, there were only two subjects per group. Given these factors, it is not surprising that a precision match across all conditions cannot be obtained with a single set of independent model parameters.

The research reported here explored only the performance consequences of g-seat cuing and we have seen an approximate performance equivalence between haptic cuing (given the appropriate drive scheme) and whole-body motion cuing). Of considerable interest is the utility of the g-seat as a device for training the pilot to use whole-body motion cues. Transfer-of-training studies regarding these sensory modalities are being evaluated at ASD/AFAMRL.

SUMMARY

A study was performed to investigate the capability of an advanced g-cuing system to provide rotational cues in a laboratory roll-axis tracking task. Six cuing algorithms were explored:

1. "Static" (visual display of roll error, no g-seat cuing)

2. "Position" (visual plus seat pan angle proportional to simulated aircraft roll angle)
3. "Velocity" (visual plus seat pan angle proportional to simulated aircraft roll rate)
4. "Acceleration" (visual plus seat pan angle proportional to simulated aircraft roll acceleration)
5. "Combined" (visual plus seat pan angle proportional to a linear combination of simulated aircraft roll angle and roll acceleration)
6. Visual plus whole-body roll-axis motion cues.

The combined algorithm was designed to match the pressure pattern that would be felt in the whole-body moving-base Roll Axis Tracking Simulator (RATS).

Performance with either the position or velocity g-cuing algorithm yielded tracking error scores that compared favorably with performance in the RATS and were substantially lower than scores obtained in the static cuing conditions. To our initial surprise, the combined algorithm provided only marginal improvement in tracking performance relative to static cuing, as did g-cuing with the pure acceleration drive law. A follow-up study indicated that subjects could perform the task well in the absence of visual cues when the g-seat was driven by the position algorithm.

A review of the literature suggested that the various haptic sensor mechanisms could be represented mathematically by (1) a lead-lag network with a zero at 0.5 and a pole at 5 rad/sec, and (2) an effective time delay 40 msec less than that associated with visual cues. When this receptor model was incorporated into the framework of the optimal control pilot model, the model was able to replicate the major experimental trends, in terms of performance scores as well as operator frequency response, with a fixed set of values for independent operator-related model parameters. Similar results were obtained for a purely informational model receptor transduction.

ACKNOWLEDGEMENT

This research was supported by the Air Force Aerospace Medical Research Laboratory under contract F33615-81-C-0515 with John B. Sinacori Associates, Inc.

REFERENCES

1. Kleinwaks, J.M. (1980). Advanced Low Cost G-cuing System (AFHRL-TR-79-62). Brooks Air Force Base, TX, Air Force Human Resources Lab. (NTIS).

2. Borah, J., Young, L.R., Curry, R.E., Albery, W.B., "Multisensory Perception Model for Application to Aircraft Simulation", NTEC IH-306, November 14-16, 1978.
3. Chambers, M.R., Andres, K.H., V. Duering, M., Iggo, A., "The Structure and Function of the Slowly Adapting Type II Mechanoreceptor in Hairy Skin", Quarterly Journal of Experimental Physiology, (1973)73, pp. 417-445.
4. Chorzempa, A., "An Attempt to Determine the Structure of the Nervous System Serving Mechanoreceptors", Biol. Cybern., 42, pp. 51-56, (1981).
5. Freeman, A.W., Johnson, K.O., "A Model Accounting for Effects of Vibratory Amplitude on Responses of Cutaneous Mechanoreceptors in Macaque Monkey", J. Physiol., (1982)323, pp. 43-64.
6. Grandori, F., Pedotti, A., "Theoretical Analysis of Mechano-to-Neural Transduction in Pacinian Corpuscle", IEEE Trans. BME-27: pp. 559-565, October 1980.
7. Gum, D.R., "Modeling of the Human Force and Motion-Sensing Mechanisms", AFHRL-TR-72-54, June 1973.
8. Horch, K.W., Tuckett, R.P., Burgess, P.R., "A Key to the Classification of Cutaneous Mechanoreceptors", The Journal of Investigative Dermatology, Vol. 69, No. 1, pp. 75-82, 1977.
9. Iggo, A., Kornhuber, H., "A Quantitative Study of C-Mechanoreceptors in Hairy Skin of the Cat", J. Physiol., (1977)271, pp. 549-565.
10. Iggo, A., Muir, A.R., "The Structure and Function of a Slowly Adapting Touch Corpuscle in Hairy Skin", J. Physiol., (1969)200, pp. 763-796.
11. Iggo, A., Ogawa, H., "Correlative Physiological and Morphological Studies of Rapidly Adapting Mechanoreceptors in Cat's Glabrous Skin", J. Physiol., (1977)266, pp. 275-296.
12. Jarvilehto, T., Hamalainen, H., Soininen, K., "Peripheral Neural Basis of Tactile Sensations in Man: II. Characteristics of Human Mechanoreceptors in the Hairy Skin", Brain Research, 219(1981), pp. 13-27.
13. Jarvilehto, H., Hamalainen, H., Kekoni, J., "Mechanoreceptive Unit Activity in Human Skin Nerves Correlated with Touch and Vibratory Sensations", In Zotterman, Y., (ed), Proc. of the International

Symposium, held at the Winner-Gren Center, January 1976, pp. 215-230.

14. Johansson, R., "Skin Mechanoreceptors in the Human Hand: Receptive Field Characteristics", pp. 159-170.
15. Ogawa, H., Morimoto, K., Yamashita, Y., "Physiological Characteristics of Low Threshold Mechanoreceptor Afferent Units Innervating Frog Skin", Quarterly Journal of Experimental Physiology, (1981)66, pp. 105-116.
16. Pubols, B.H., "Factors Affecting Cutaneous Mechanoreceptor Response. I. Constant-Force Versus Constant-Displacement Stimulation", J. Neurophysiology, Vol. 47, No. 3, March 1982, pp. 515-529.
17. Vedel, J.P., Roll, J.P., "Response to Pressure and Vibration of Slowly Adapting Cutaneous Mechanoreceptors in the Human Foot", Neuroscience Letters, 34(1982), pp. 289-294.
18. Woodworth, R.S., and Schlosberg, H., Experimental Psychology, Revised, Holt, New York, 1956.
19. Boulter, L.R., "Attention and Reaction Times to Signals of Uncertain Modality", J. Expt. Psych: Human Perception and Performance, 3:379-388, August 1977.
20. Levison, W.H., "Development of a Model for Human Operator Learning in Continuous Estimation and Control Tasks", BBN Report No. 5331, Bolt Beranek and Newman, Inc., Cambridge, MA, September 1983.